The 2009 IEEE/RSJ International Conference on
Intelligent Robots and Systems
October 11-15, 2009 St. Louis, USA

Asymmetric flapping for a robotic fly using a hybrid power-control actuator

Benjamin M. Finio, *Student Member, IEEE*, Brandon Eum, Christopher Oland
and Robert J. Wood, *Member, IEEE*

***Abstract*— This paper continues the exploration of the design space for an insect-sized autonomous flapping-wing MAV with the goal of stable hovering. Previous work has focused on the use of a large primary power actuator to generate flapping motion and smaller "control" actuators to asymmetrically alter wing kinematics. Here a new iteration of this concept is presented, merging the two actuator types to create a "hybrid" power-control actuator. Kinematic and dynamic models for wing motion are presented, and the predictions of these models are compared to experimental results from a prototype design. Controllable asymmetry in wing kinematics can be mapped into controllable body torques via an aerodynamic model, and this information can be used for the generation of control laws for stable hover and eventually highly agile aerial vehicles.**

I. Introduction

Recently there has been increased research in the area of flapping-wing micro air vehicles (MAVs), typically defined to have a wingspan of less than 15cm [1], because of the advantages they may demonstrate over their traditional fixed-wing counterparts. Inspired by extremely agile natural flyers, flapping-wing MAVs will be useful for exploration in confined spaces such as urban environments, indoor areas, and collapsed buildings - areas typically off-limits to larger flying vehicles.

There are numerous examples of MAVs inspired by insects, small birds or bats [2], [3], [4], [5], [6]. Insect-scale MAVs (Fig. 1) were first developed at Berkeley's Biomimetic Millisystems Lab [7], [8], [9], and continued development at the Harvard Microrobotics Lab [10], [11], [12]. Unique fabrication and actuation challenges at the insect scale have been met through the development of novel meso-scale manufacturing techniques [13] and the use of high energy density piezoelectric actuators [14] respectively. Miniaturization of power electronics to meet the high voltage requirements of piezoelectric actuators is an ongoing research area [15], [16].

Another unique challenge in flapping-wing MAV design is the reconstruction of insect-like wing kinematics. Insects possess dozens of muscles and redundant control inputs [5], and it is a daunting challenge to reproduce structures on the scale and complexity of a Dipteran (fly) thorax. Instead, many MAV designs rely on the use of parallel mechanisms to produce primary flapping motion, and either rely on passive dynamics or additional actuators to drive wing rotation about the spanwise axis (hereafter referred to as *stroke angle* ϕ and *rotation angle* ψ respectively).

The authors are with the School of Engineering and Applied Sciences, Harvard University, Cambridge, MA 02138 bfinio@fas.harvard.edu

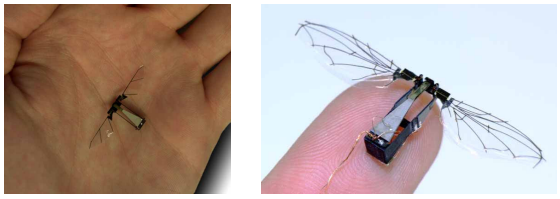

Fig. 1. Two previous iterations of the Harvard Microrobotic Fly.

Without the use of thrust vectoring via a device such as a tail rudder, asymmetric control of wing kinematics is required to generate asymmetric aerodynamic forces, and thus body torques.

The most immediately apparent solution to this problem is to have separate power actuators for each degree of freedom (two per wing, four total). However, this design can be costly in terms of overall weight budget, a critical concern for insect-sized MAVs, due to potentially unnecessary (and heavy) power actuators. An approach that has proven more successful is to use a single power actuator to generate primary flapping motion while relying on passive dynamics for wing rotation. We have previously demonstrated a thoracic topology which combines the efficiency of passive rotational dynamics with small, low-power control actuators to achieve asymmetric wing motions [17]. Here we expand upon this concept by introducing a "hybrid" 2-DOF power-control actuator.

II. Mechanical Design

The original Harvard Microrobotic Fly design consisted of a single power actuator and symmetric 1-DOF four-bar transmission, which converts a linear input δ_1 from the actuator to rotational motion ϕ of the wings (Fig. 2a). Pitch torques could be generated by shifting the DC value of the power actuator signal (Fig. 3b), but asymmetric wing motion, thus generation of roll or yaw torques, was impossible. The design introduced in [17] made use of two smaller "control" actuators in addition to the primary power actuator. These actuators introduced control inputs δ_2 and δ_3, allowing movement of the previously grounded wing pivots and asymmetric modulation of wing kinematics (Fig. 2b). The ability to asymmetrically modulate stroke amplitude allows controllable generation of yaw torques (Fig. 3c). This design was inspired by thoracic mechanics of Dipteran insects, where large indirect power muscles generate the primary flapping motion, and small control muscles at the base of the wing fine-tune wing kinematics for steering purposes

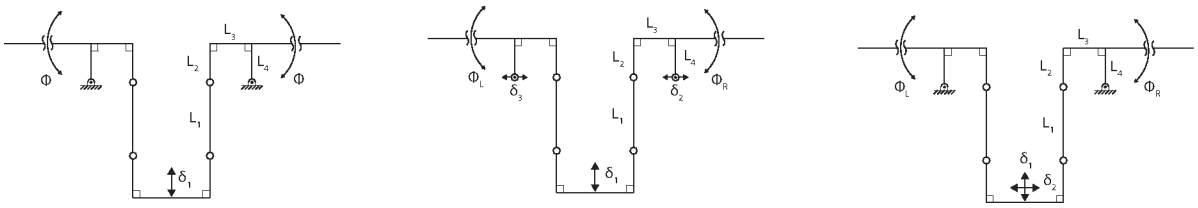

Fig. 2. The original 1-DOF transmission design with only one power actuator input and no control inputs (a), a 3-DOF design that uses a single power actuator and two control inputs (b), and the newest 2-DOF design which uses a coupled power-control input (c). Note that in (a) and (b), the central link of the transmission is constrained to move vertically.

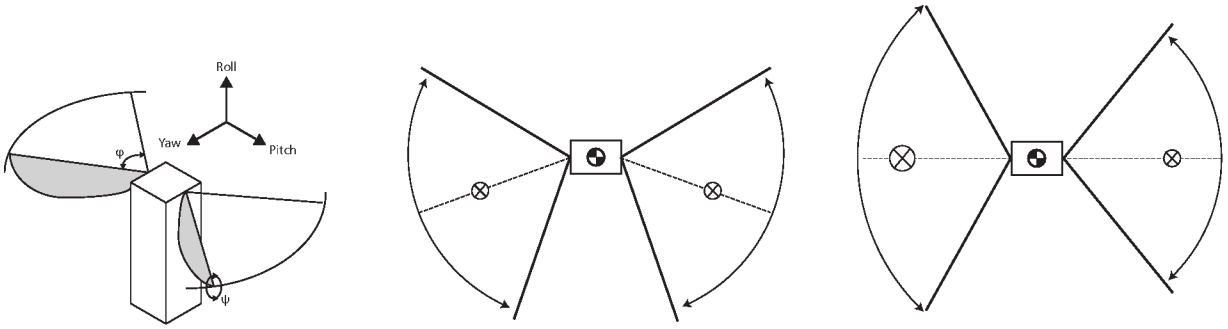

Fig. 3. Definition of the stroke parameters ϕ and ψ as well as the three body rotation axes (a). Pitch torques can be generated by symmetrically moving the mean stroke angle for each wing forward or backward (b), and yaw torques can be generated by asymmetrically changing stroke amplitude (c).

[18]. The design presented in this paper uses a coupled 2-DOF power-control actuator structure, which allows the central link of the transmission to be moved orthogonal to the primary actuation mode (Fig. 2c). This permits a coupled change in stroke angles of the left and right wings, ϕ_L and ϕ_R.

The motion of the distal tip of a cantilevered piezoelectric bimorph actuator acts as the input to the transmission. The geometry of the actuators can be selected to give desired force, displacement and energy density characteristics. Maximizing energy density is vital for MAVs since weight budget is an enormous concern, and force and displacement must be selected to give the desired wing motion based on expected aerodynamic loading and transmission geometry. The complete model for design and optimization of the actuators is presented in [14]. The "hybrid" power-control actuator (Fig. 4) consists of two bimorphs connected by a 90° angle bracket, and requires four electrical inputs: two constant voltages (bias and ground), shared between the bimorphs, and two independent signal voltages (power and control). Voltages required to drive the actuators are typically in the range of 200-300V. While on-board batteries are expected to provide only about 3V, miniaturized high-voltage amplifier circuits have been developed [16] for the purpose of allowing such batteries to be used for piezoelectrically driven microrobots with stringent weight requirements.

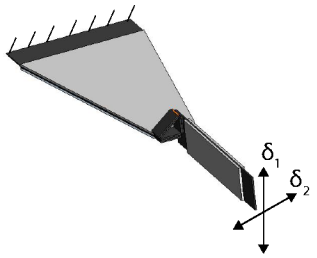

Fig. 4. A hybrid power-control actuator, consisting of two piezoelectric bimorphs connected by a 90° angle bracket.

Transmission geometry selection to optimize both transmission ratio (ratio of stroke amplitude to power actuator displacement) and control power (*change* in stroke amplitude per unit control actuator displacement, for a fixed power actuator input) are presented in [11] and [17] respectively. Optimization of these parameters allows maximal wing movement for a given actuator input (or, conversely, minimizes required actuator displacement for desired wing motion), thus increasing the propulsive efficiency of the vehicle. Based on these previous analyses, transmission link lengths (as labeled in Fig. 2) are selected to be $L_1 = 400\mu$m, $L_2 = 300\mu$m, $L_3 = 300\mu$m, and $L_4 = 450\mu$m.

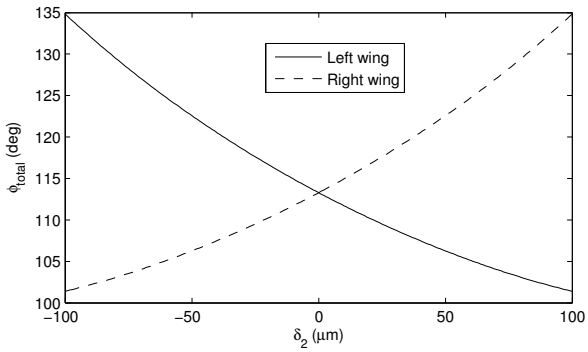

Fig. 5. Kinematic model for stroke amplitude of the left and right wings plotted over a range of control actuator motion, for a fixed power actuator input ($\delta_1 = \pm 300\mu m$).

III. Kinematics

The stroke angle ϕ can be written as a function of transmission geometry and actuator inputs δ_1 and δ_2 as follows:

$$\phi = acos\left(\frac{(L_y-\delta_1)^2 + C_1}{C_2\sqrt{L_x^2+(L_y-\delta_1)^2}}\right) + atan\left(\frac{L_x}{L_y-\delta_1}\right) + atan\left(\frac{L_2-L_4}{L_3}\right) - \frac{\pi}{2} \quad (1)$$

where $L_x = L_3 + \delta_2$ or $L_x = L_3 - \delta_2$ for the left and right wings, respectively, and

$$L_y = L_1 + L_2 - L_4 \quad (2)$$

$$C_1 = L_3^2 + (L_2 - L_4)^2 - L_1^2 + L_x^2 \quad (3)$$

$$C_2 = 2\sqrt{L_3^2 + (L_2 - L_4)^2} \quad (4)$$

Using (1), the effect of control actuator movement on wing stroke amplitude can be predicted (Fig. 5). In the control actuator's neutral position, the stroke amplitudes of the left and right wings are equal and thus there will be no net yaw torque. When the control actuator moves in either direction, it increases one wing's stroke amplitude while decreasing the other. This difference in amplitude will create different average lift forces on each wing, and thus a yaw torque (as shown above in Fig. 3).

IV. Dynamics

The kinematic model assumes the actuator acts as a linear displacement source. It is more realistic to model the dynamic system and include the actuator as a force source. This also allows the study of resonant effects, which cannot be done with a purely kinematic model. An Euler-Lagrange energy formulation can be used to derive the second order differential equation of motion for the system. Examples of this derivation are presented in [17] and [19] and will not be repeated in full here, however a brief explanation is warranted.

The actuator is treated as a sinusoidally applied force source in parallel with a linear spring (due to internal elastic deformation of the actuator). Wing inertia is dominant over other components of the system and thus is included in the model. An aerodynamic damping force is applied at the center of pressure of the wings (a distance r_{cp} from the wing base). The aerodynamic damping is based on a quasi-steady blade element model [20]. Finally, to reduce the system to 1-DOF, the rotation angle ψ is correlated to the stroke angle ϕ from empirical observation (in practice, ψ is observed to be approximately 45° at the mid-stroke and 90° at the ends of the stroke). The dynamic model is summarized in Fig. 6. Note that while the actuator terms are expressed in the power actuator coordinate δ_1 and the aerodynamic terms are written in the wing coordinate ϕ, δ_1 and ϕ are related explicitly via (1) so either can be selected as a generalized coordinate for use with the Euler-Lagrange formulation.

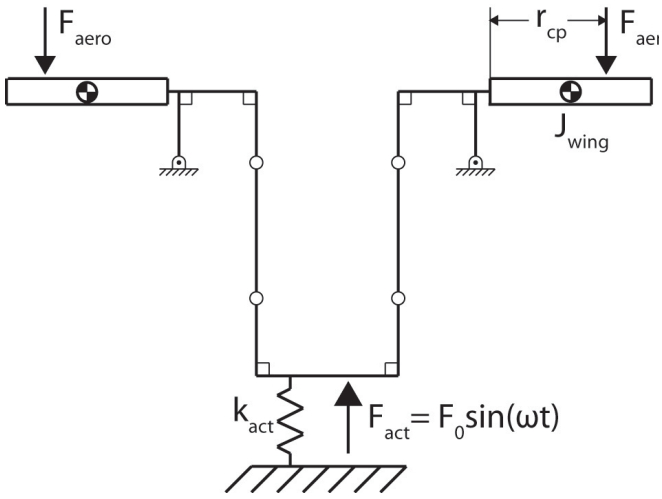

Fig. 6. Diagram for the dynamic model of the actuator, transmission and wing system (not to scale).

The dynamic model can be applied in a manner similar to the kinematic model in order to determine the effect of control actuator position on wing motion, given a power actuator signal (in this case a force instead of a displacement). Numerically solved wing trajectories are shown in Fig. 7 for three different control actuator positions. As expected, the dynamic model shows that control actuator motion will create asymmetric wingstroke amplitudes. This is illustrated in Fig. 8, which shows stroke amplitudes for the left and right wings as a function of both power actuator frequency and control actuator position. The control actuator motion has the same effect as predicted by the kinematic model (increased $\phi_{R,tot}$ and decreased $\phi_{L,tot}$ for $\delta_2 > 0$, vice versa for $\delta_2 < 0$), but here we also see that there is a clear resonant peak for wing amplitude. However, the *difference* between stroke amplitudes depends primarily on control actuator position and is fairly independent of drive frequency (Fig. 9).

Most important from a control standpoint, the blade-element aerodynamic model can be used to calculate the lift force on each wing. This allows calculation of net body torques, and thus angular acceleration using a rough first-order approximation that ignores any rotational aerodynamic damping on the body. Predicted body torques are on the order of 1mN·mm. This is consistent with dynamic simulations

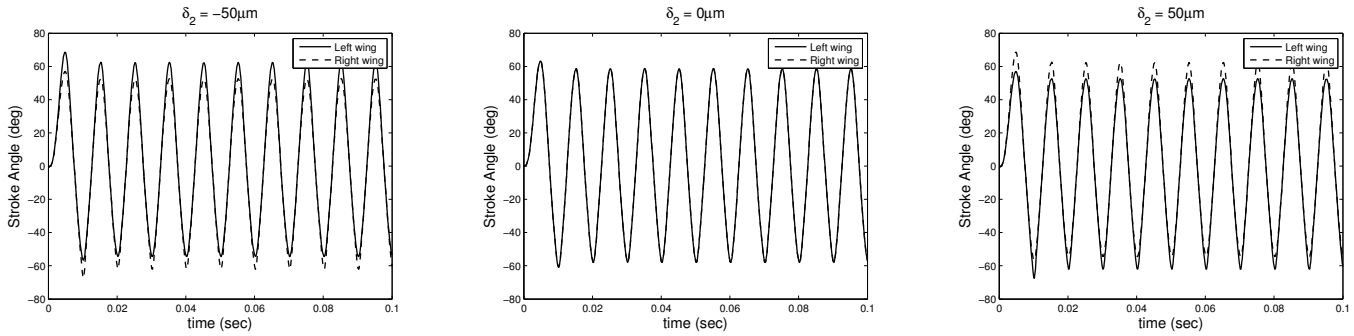

Fig. 7. Numerical solutions for wing trajectory as a function of time for three different control actuator positions. As predicted with the kinematic model, the dynamic model shows that the control actuator will create an asymmetry in stroke amplitude.

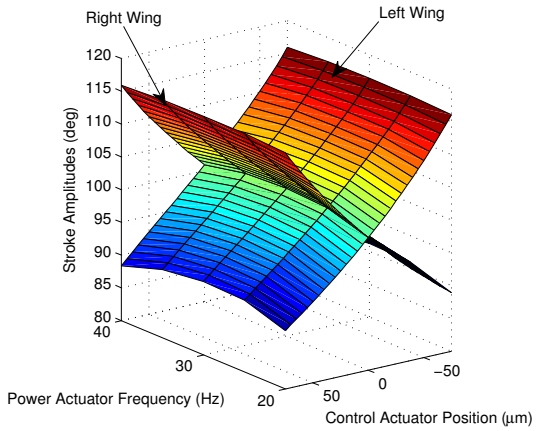

Fig. 8. Results of numerical simulations showing left and right wing stroke amplitudes as a function of both power actuator frequency and control actuator position. A shallow resonant peak in stroke amplitude is evident around 30Hz.

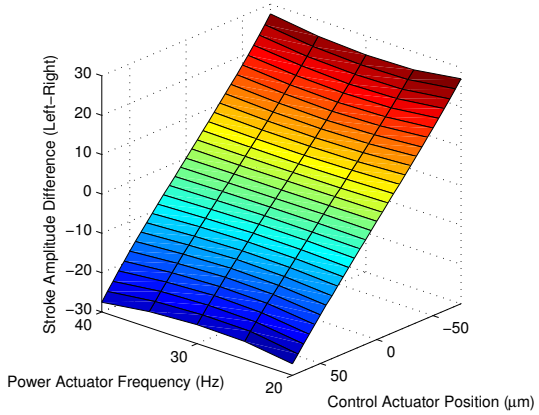

Fig. 9. Numerical simulations showing the *difference* between wing stroke amplitudes.

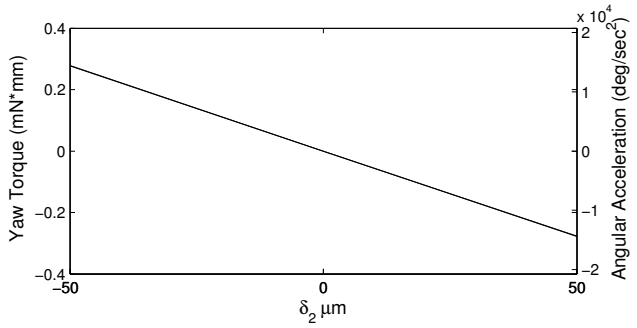

Fig. 10. Net yaw torques and resulting angular accelerations as a function of control actuator position (at constant power actuator frequency), from numerical simulations.

from [17] and torque measurements of tethered insects [21]. Due to the robotic fly's low mass moment of inertia about the yaw axis (1.1g·mm^2 as calculated with a Solidworks model), this allows for high angular accelerations on the order of thousands of deg/sec^2 (Fig. 10). Previous work has shown that rapid turns during insect flight are actually inertia-dominated and not viscous-dominated [22], so ignoring rotational aerodynamic damping in this calculation is not an unreasonable assumption.

V. Experiment

While kinematic and dynamic models are useful as design tools and for conceptualizing different control strategies, experimental validation of their predictions is vital. Inaccuracies arise in both the kinematic and dynamic modeling approaches that limit their applicability. For example, the kinematic model assumes the transmission structure consists of rigid links connected by ideal revolute joints, while in reality there is a finite compliance in the mechanism and the flexure joints may experience axis drift. It also assumes perfect geometric construction (exact 90° angles, symmetric alignment etc.), which is currently difficult to achieve when manufacturing devices at such a small scale. The dynamic model is limited both due to difficulties in accurately predicting actuator force and stiffness, and assumptions inherent in the quasi-steady aerodynamic model, e.g. neglecting spanwise flow along the wing, vortex shedding, wake capture, and

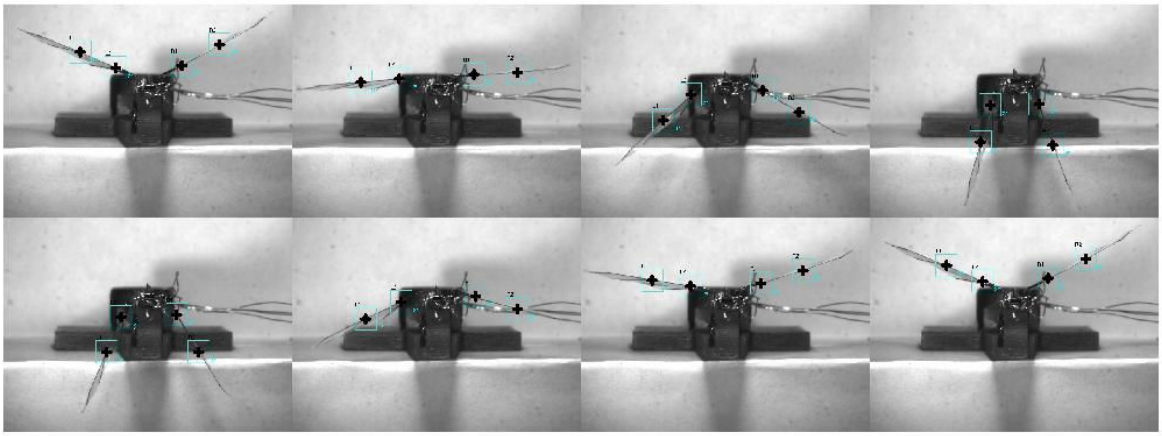

Fig. 11. Sample screenshots from ProAnalyst software showing wing markers being tracked through a video. Stroke angles are automatically calculated with the software based on marker positions.

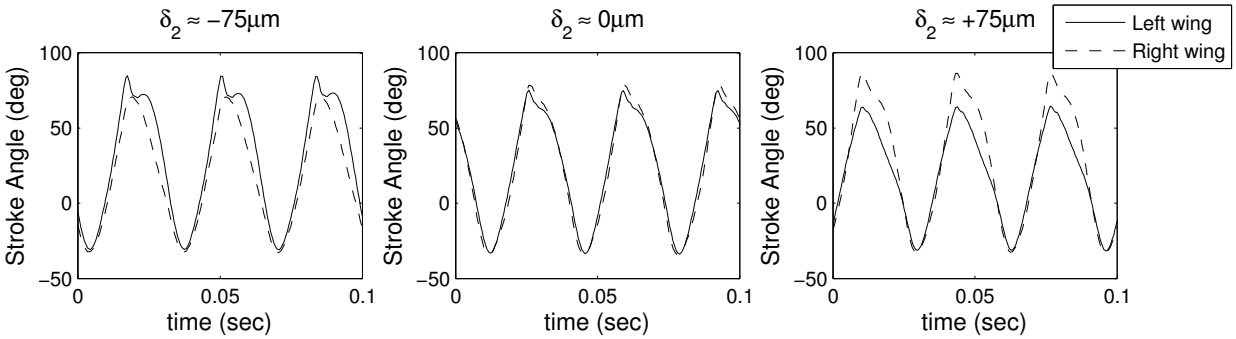

Fig. 12. Wing trajectories extracted from videos using the ProAnalyst software. While not perfectly symmetric due to minor manufacturing defects, the resulting wing motion is comparable to that of the dynamic simulations as shown in Fig. 7.

other aerodynamic effects that are known to be beneficial to insect lift generation.

Therefore, a test device was constructed to empirically determine the effects of control actuator motion on wing trajectory (Fig. 13). The structure was designed with oversized actuators and built on a rapid-prototyped acrylic base in order to serve as a robust test bed and proof of concept. Future designs will incorporate optimal-energy density actuators onto a lightweight carbon fiber airframe.

Two retroreflective markers (small pieces cut from Reflexite tape [23]) were placed on the leading edge of each wing. Note that these markers significantly increase the inertia of the wings, which is compensated for by the oversized power actuator. This has the effect of significantly lowering the system resonant frequency (about 30Hz for this test structure, compared to 110Hz in previous designs). Since the markers are used only for data collection and serve no other functional purpose, they would not be required on a final design.

A high-speed camera was oriented toward the leading edge along with two fiber-optic light sources for illumination (Fig. 14). With a black background, this allowed filming of high-contrast video in order to automatically track the wing markers. Automated tracking was performed with 2D image analysis software (ProAnalyst [24]). Sample video frames (with a white background for image clarity and illustration purposes) with tracked markers are shown in Fig. 11, and sample wing trajectories extracted for three different videos are shown in Fig. 12.

Tests were performed over a range of control actuator positions (-75μm to +75μm) and power actuator frequencies (20Hz to 40Hz) while holding power actuator amplitude constant. The total and difference in stroke amplitudes are presented in Fig. 15 and Fig. 16 respectively. As predicted by the kinematic and dynamic models, control actuator motion has a large effect on relative wing motion. While drive frequency does have an effect on the individual stroke amplitude of each wing, it has little effect on the *difference* in amplitudes. A "slice" of the data from Fig. 15 at 30Hz is shown in Fig. 17. This plot makes the asymmetry of the data more evident - changes in wing amplitude are not perfectly symmetric about the control actuator's neutral position, as predicted by the kinematic or dynamic models. This can likely be attributed to a manufacturing asymmetry in the transmission or actuator, and highlights the need for

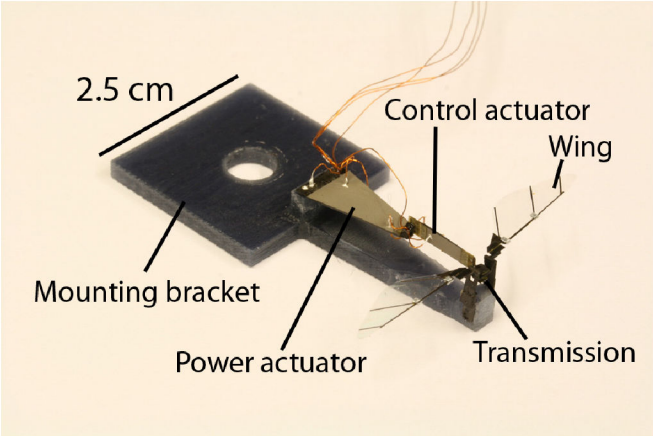

Fig. 13. The complete test device. The hybrid actuator and transmission structure are mounted to rapid-prototyped rigid acrylic base. Retroreflective markers are placed on the leading edge of each wing in order to enhance automated data collection capabilities.

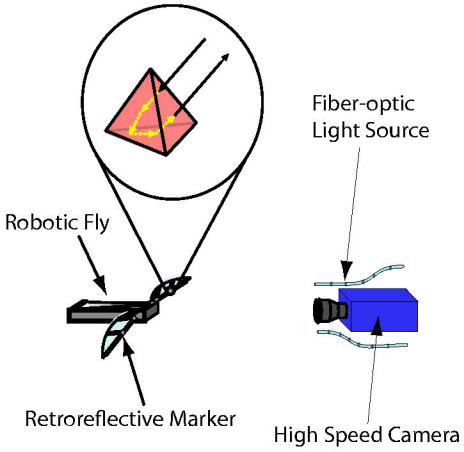

Fig. 14. Schematic of the test setup. Retroreflective wing markers and fiber optic illuminators were used in order to facilitate automated tracking of the wing trajectory (not to scale).

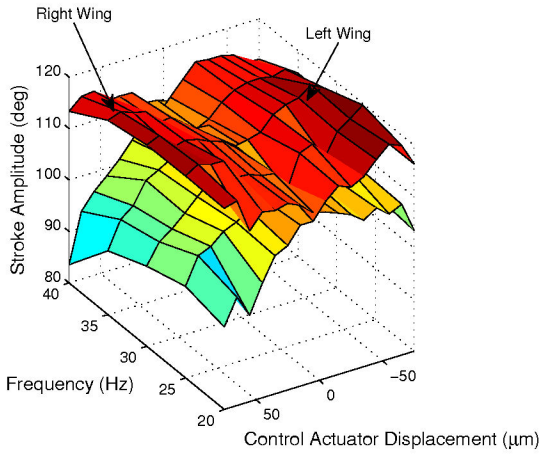

Fig. 15. Experimental data showing total stroke amplitude for the left and right wings. The data is characterized by a broad resonant peak and a strong dependence on control actuator position.

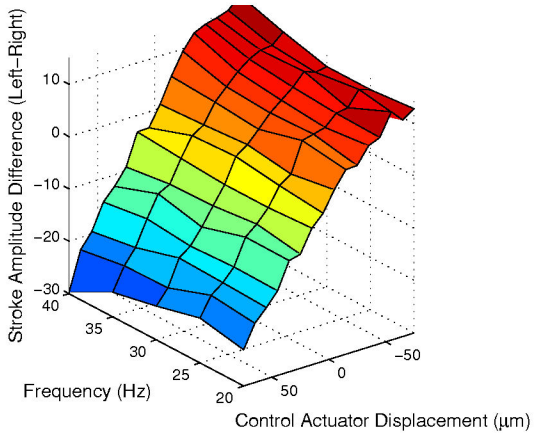

Fig. 16. Experimental data showing difference in stroke amplitude $\phi_{total,L} - \phi_{total,R}$ as a function of both control actuator displacement and power actuator drive frequency.

mechanization of the micro-assembly process. Increasing the accuracy, repeatability and level of automation of our assembly process is an ongoing research area.

The oversized actuators used on the test structure allow for very large differences in stroke amplitude, exceeding 30°. Data on actual insects shows that the difference in stroke amplitudes required to generate sufficient body torques for rapid turns is "remarkably subtle" [22], thus the values observed here are beyond what is necessary for typical maneuvers. This allows the size of the control actuator to be decreased in order to better meet the vehicle weight budget; however, this must be balanced with the decrease in maximum possible body torques that will result. Final vehicle design will require an optimization of thrust-to-weight ratio and maneuverability through proper actuator sizing.

Most importantly, these results function as proof that the hybrid power-control actuator concept can be implemented to create controlled asymmetries in wing motion. Improved kinematic and dynamic modeling, coupled with more repeatable and reliable manufacturing techniques, will result in increased correlation between theoretical predictions and experimental results. Aerodynamic modeling and torque measurements can be used to map control actuator signals to resultant net body torques, and this information can be used for the development of control laws for stable hovering. Note that while a freely flying body has six total degrees of freedom (three translational, three rotational), direct control of all six DOF is not required to allow stable hover. For example, many insects can control the magnitude and direction of their net thrust vector, but cannot directly produce sideways or forward aerodynamic forces. In steady hover, the net aerodynamic force is purely vertical, to accelerate

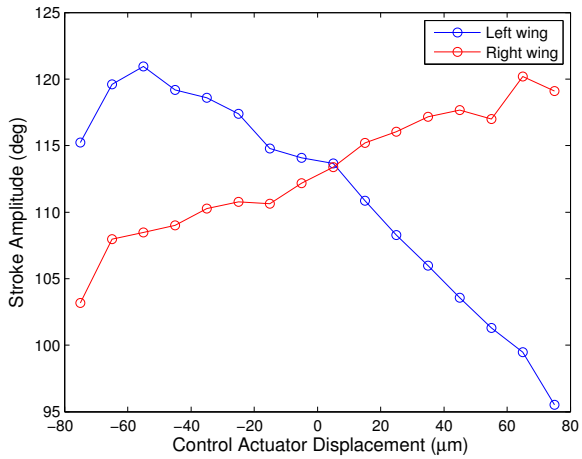

Fig. 17. Total stroke amplitudes of the left and right wings plotted against the applied control actuator displacement, at a constant power actuator frequency of 30Hz.

forward or laterally the insect will tilt in that direction, giving a horizontal component to the aerodynamic force vector [25]. Similarly, the design presented here can control two of the three rotational degrees of freedom and the magnitude of thrust (by modulating stroke frequency and amplitude), sufficient for stable hover. Additional controlled body degrees of freedom may be desirable to allow for a more agile vehicle.

In addition to controllable body degrees of freedom, in order to hover a thrust to weight ratio greater than unity is also required. The minimal design presented in [10], [11], [13] had a mass of 60mg and a 2:1 thrust:weight ratio. This leaves an absolute maximum of 60mg for additional payload (control actuators, power electronics, sensors etc.). For a larger (or smaller) desired payload, vehicle wing area and wingbeat frequency (and thus resultant wing loading and required actuator size) must be scaled appropriately; for insects wing area scales with body mass$^{0.71}$ and wingbeat frequency scales with mass$^{-0.24}$ [25].

VI. Conclusions and Future Work

This paper has presented a control method for generating yaw torques on a microrobotic insect platform. A "hybrid" power-control actuator is used to provide primary flapping power while simultaneously asymmetrically modulating wing kinematics. Experimental results from a test platform show reasonable agreement with kinematic and dynamic predictions, but also highlight the need for higher fidelity modeling and more repeatable manufacturing processes. Next steps include integration of this technique into a flightweight platform (Fig. 18), as well as the exploration of other control methods. These include, but are not limited to: separate power and control actuators [17]; a hybrid bending-twisting power-control actuator; more traditional approaches, such as thrust vectoring with flaps; and more novel approaches, such as using active materials with variable elasticity properties to dynamically alter the system response. Such techniques will be explored and applied in order to help meet the demanding challenges of sub-100 milligram flying vehicles, to move toward the ultimate goal of fully autonomous flight.

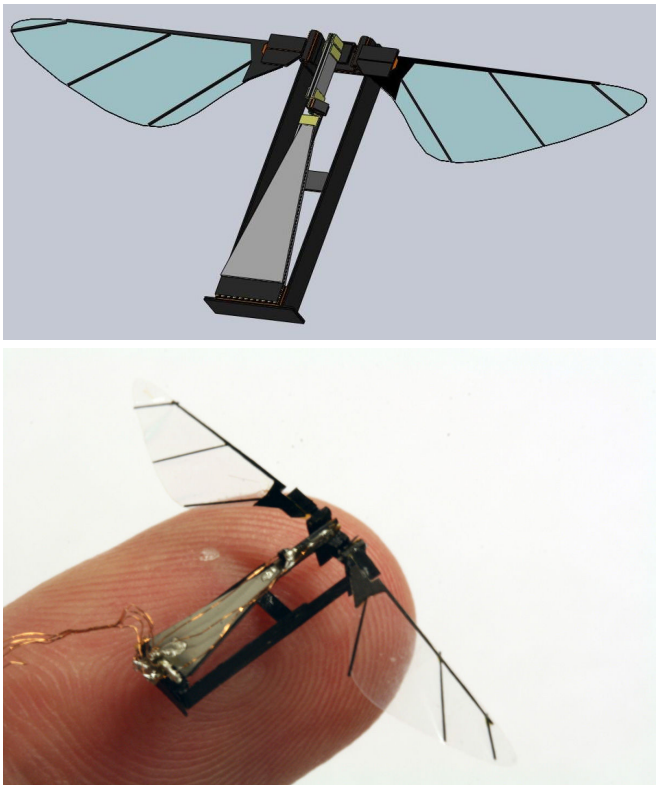

Fig. 18. A 3D CAD model of a flightweight design utilizing the hybrid actuator structure (top), and a next-generation prototype (bottom).

VII. Acknowledgements

This work was supported in part by the Army Research Laboratory (award number W911NF-08-2-0004) and the National Science Foundation (award number CMMI-07466 38). Any opinions, findings and conclusions or recommendations expressed in this material are those of the authors and do not necessarily reflect those of the National Science Foundation.

References

[1] M. Platzer and K. Jones, "Flapping wing aerodynamics–progress and challenges," *AIAA Journal*, vol. 46, no. 9, pp. 2136–2149, 2008.

[2] H. Tanaka, K. Hoshino, K. Matsumoto, and I. Shimoyama, "Flight dynamics of a butterfly-type ornithopter," *IEEE/RSJ International Conference on Intelligent Robots and Systems*, pp. 2706–2711, 2005.

[3] R. Madangopal, G. Student, Z. Khan, and S. Agrawal, "Biologically Inspired Design Of Small Flapping Wing Air Vehicles Using Four-Bar Mechanisms And Quasi-steady Aerodynamics," *Journal of Mechanical Design*, vol. 127, p. 809, 2005.

[4] G. Bunget and S. Seelecke, "BATMAV: a biologically-inspired micro-air vehicle for flapping flight: kinematics and actuation," in *Proceedings of SPIE*, vol. 6928. SPIE, 2008, p. 69282F.

[5] A. Conn, S. Burgess, and C. Ling, "Design of a parallel crank-rocker flapping mechanism for insect-inspired micro air vehicles," *Proceedings of the Institution of Mechanical Engineers, Part C: Journal of Mechanical Engineering Science*, vol. 221, no. 10, pp. 1211–1222, 2007.

[6] J. Park and K. Yoon, "Designing a Biomimetic Ornithopter Capable of Sustained and Controlled Flight," *Journal of Bionic Engineering*, vol. 5, no. 1, pp. 39–47, 2008.

[7] R. Fearing, K. Chiang, M. Dickinson, D. Pick, M. Sitti, and J. Yan, "Wing transmission for a micromechanical flying insect," in *IEEE International Conference on Robotics and Automation*, vol. 2, 2000, pp. 1509–1516.

[8] M. Sitti, "PZT actuated four-bar mechanism with two flexible links for micromechanical flying insect thorax," in *IEEE International Conference on Robotics and Automation*, vol. 4, 2001, pp. 3893–3900.

[9] S. Avadhanula, R. Wood, D. Campolo, and R. Fearing, "Dynamically tuned design of the MFI thorax," in *IEEE International Conference on Robotics and Automation*, vol. 1, 2002, pp. 52–59.

[10] R. Wood, "Liftoff of a 60mg flapping-wing MAV," in *IEEE/RSJ International Conference on Intelligent Robots and Systems*, 2007, pp. 1889–1894.

[11] ——, "Design, fabrication, and analysis, of a 3DOF, 3cm flapping-wing mav," in *IEEE/RSJ International Conference on Intelligent Robots and Systems*, 2007, pp. 1576–1581.

[12] ——, "The first takeoff of a biologically inspired at-scale robotic insect," in *IEEE Transactions on Robotics*, vol. 24, no. 2, 2008, pp. 341–347.

[13] R. Wood, S. Avadhanula, R. Sahai, E. Steltz, and R. Fearing, "Microrobot Design Using Fiber Reinforced Composites," *Journal of Mechanical Design*, vol. 130, pp. 52 304–52 315, 2008.

[14] R. Wood, E. Steltz, and R. Fearing, "Optimal energy density piezoelectric bending actuators," *Sensors and Actuators A: Physical*, vol. A 119, pp. 476–488, 2005.

[15] M. Karpelson, G. Wei, and R. Wood, "A review of actuation and power electronics options for flapping-wing robotic insects," in *Robotics and Automation, 2008. ICRA 2008. IEEE International Conference on*, 2008, pp. 779–786.

[16] ——, "Milligram-Scale High-Voltage Power Electronics for Piezoelectric Microrobots," in *Robotics and Automation, 2009. ICRA 2009. IEEE International Conference on*, 2009.

[17] B. Finio, J. Shang, and R. Wood, "Body Torque Modulation for a Microrobotic Fly," in *Robotics and Automation, 2009. ICRA 2009. IEEE International Conference on*, 2009, pp. 3449–3456.

[18] M. Dickinson and M. Tu, "The function of dipteran flight muscle," *Comp. Biochem. Physiol.*, vol. 116A, no. 3, pp. 223–238, 1997.

[19] S. Avadhanula, "Design, fabrication and control of the micromechanical flying insect," Ph.D. dissertation, University of California, Berkeley, 2006.

[20] J. Whitney, "Aeromechanics of Passive Rotation in Flapping Flight," 2009, under review, Journal of Fluid Mechanics.

[21] S. Fry, R. Sayaman, and M. Dickinson, "The aerodynamics of hovering flight in Drosophila," *Journal of Experimental Biology*, vol. 208, no. 12, pp. 2303–2318, 2005.

[22] S. Fry and M. Dickinson, "The aerodynamics of free-flight maneuvers in drosophila." *SCIENCE*, vol. 300, no. 5618, pp. 495–498, 2003.

[23] "About reflexite americas - technology," http://www.reflexiteamericas.com/technology.htm.

[24] "Xcitex products and solutions," http://xcitex.com/html/products.php.

[25] R. Dudley, *The biomechanics of insect flight: form, function, evolution*. Princeton University Press, 2000.